Biophysical Journal, Volume *119*

Supplemental Information

Mechanical Forces Regulate Asymmetric Vascular Cell Alignment

Xin Cui, Jie Tong, Jimmy Yau, Apratim Bajpai, Jing Yang, Yansong Peng, Mrinalini Singh, Weiyi Qian, Xiao Ma, and Weiqiang Chen

SUPPORTING METHODS

1. Thin-sheet finite element method (FEM) model and intercellular force calculation

We modelled the cellular monolayer as a linearly elastic and isotropic substance and solved for intercellular forces under the continuum hypothesis using a FEM model upon the TFM measured traction force data (26, 30). In such a system traction forces are a result of internal forces according to Newton's law (35). Hence a relationship between traction forces and internal sheet forces can be established as:

$$\frac{d\sigma_{ij}}{dj} = -h * T_j, over\ the\ entire\ region\ of\ interest \tag{1}$$

where, Tj is the traction component in the j direction measured by traction force microscopy. Stresses in a monolayer are related to the strains as:

$$\sigma_{ij} = \frac{\mathrm{E}}{1-v} * [\varepsilon_{ij} + \frac{1}{1-2v} * \varepsilon_{ll} * \delta_{\mathrm{ij}}] \tag{2}$$

where, ε_{ij} is the strain tensor, σ_{ij} is the stress field, E is the Young's modulus of the elastic material, and v is the Poisson's ratio. In our model, E = 16.2 kPa and v = 0.499.

Strain in the sheet is related to the displacement as follows:

$$\begin{bmatrix} \varepsilon_{xx} \\ \varepsilon_{yy} \\ \varepsilon_{xy} \end{bmatrix} = \begin{bmatrix} \frac{du_x}{dx} \\ \frac{du_y}{dy} \\ \frac{1}{2} * \left(\frac{du_x}{dy} + \frac{du_y}{dx}\right) \end{bmatrix} \tag{3}$$

A customized MATLAB code was used to solve the partial differential equations (PDEs) to infer the sheet forces acting inside a cellular colony with a free boundary condition, along the internal and external boundary of the colony.

$$\sigma_{ij}.n_j = 0 \tag{4}$$

Subsequently the internal forces inside the colony are calculated as:

$$f_{1,2} = -\int \sigma dl\ , over\ the\ boundary, 1 \rightarrow 2 \tag{5}$$

The vector *dl* is perpendicular to the cell boundary and points towards the cell center.

2. Computational modelling of the force distribution in micropatterned cellular monolayer

A finite element method (FEM) based model of the cellular monolayer was constructed using Autodesk Fusion 360 to analyze the mechanical force distribution, using a two-component setup similar to one described in a previous study (32). Briefly a bi-layer model was constructed to depict the shape and features of the various micropatterned monolayers, with a constrained passive layer (bottom surface) representing the substrate and a contractile layer representing the cellular monolayer. Thermal force was induced in the system by creating a thermal gradient between the contractile and the passive layer. Both the contractile layer (Height: 50 μm, Thermal conductivity: 0.2275 $W \cdot m^{-1} \cdot K^{-1}$, Young's modulus: 16.2 kPa, Poisson's ratio: 0.499, Coefficient of expansion: 0.0001 K^{-1}) and the passive layer (Young's modulus: 16.2 kPa, Poisson's ratio: 0.499) were modelled as isotopically elastic substances. We simulated monolayer contraction by using a temperature drop of 50 K between the contractile and passive layer. All simulations, were performed with finite-element mesh density corresponding to a spacing of 5-15 μm per node. Force and strain tensors were calculated throughout the structures. The von Mises force at the bottom fixed surface was reported. Convergence was confirmed by varying mechanical properties of materials and mesh densities.

3. Computational modelling of mechanical force-mediated asymmetric cell alignment in the micropatterned vascular monolayer using a coherent angular movement-based model

We adopted a model based on the concept of coherent angular movement (CAM) as described in a previous study (31) to explore the effect of mechanical forces in guiding the cell asymmetric alignment in confined patterns. This model uses the inherent mobility of cell to simulate the cell-ECM traction force and uses intercellular interactions and an arresting wall force to simulate the cellular motion in a confined cellular monolayer.

The dynamics of CAM was modelled by using a cell center based mechanical model, where the cellular bulk was represented using its center of mass. Each cell has a preferred direction of motion given by n_i, and an inherent velocity v_0. The polarization coordination constant $1/\tau$ (non-dimensional value of 0.5) was used to determine the tendency of cell's polarization to rotate and align with the migration velocity vector. Each cell was assumed to be connected to the neighbor cells by a spring and the contacts had an undeformed length R_{eq}. The maximum distance between neighbor cells which was indicative of the maximum size of the cell was taken as R_0. For all the

simulations, parameters are non-dimensional. Based on the distance between the cells, each cell experiences adhesive, repulsive, or no force along the vector connecting the cells, given by the following equation.

$$\mathbf{F}(\mathbf{r}_i, \mathbf{r}_j) = \mathbf{e}_{ij} \times \begin{cases} F_{\text{rep.}} \frac{d_{ij} - R_{\text{eq.}}}{R_{\text{eq.}}} & , d_{ij} < R_{\text{eq.}} \\ F_{\text{adh.}} \frac{d_{ij} - R_{\text{eq.}}}{R_0 - R_{\text{eq.}}} & , R_{\text{eq.}} \leq d_{ij} \leq R_0 \\ 0 & , R_0 < d_{ij} \end{cases} \tag{6}$$

Here, r_i, r_j are the coordinates of the center of the cells, $d_{ij} = |r_i - r_j|$, $e_{ij} = (r_i - r_j)/ d_{ij}$, F_{rep} and F_{adh} are the constants of repulsive and adhesive forces respectively, which are used as intercellular force. In all simulations, F_{rep} equals F_{adh}. For the numerical calculation in different patterns, $F_{rep} = F_{adh} = 1$ for the pattern D = 1, and $F_{rep} = F_{adh} = 4$ for the patterns D = 0.75, 0.55, 0.35.

Teo wall forces, F_{wall} were applied both boundaries to ensure the confinement of cell in the pattern, whereas an inward wall force on the outer pattern boundary and an outward wall force on the inner pattern boundary were set to stop the cell from leaving the outer pattern boundary. The cell-matrix traction force at different position in the pattern was varied as a negative exponential function of the distance between cell from each boundary, was given by F_w, and calculated by the following equation.

$$\mathbf{F}_w(d_{iw}) = \mathbf{n}_w \begin{cases} -F_{\text{wall}} \exp\left(-\frac{2d_{iw}}{R_0}\right), & d_{iw} < R_0, \\ 0, & R_0 < d_{iw}, \end{cases} \tag{7}$$

Here, F_{wall} is the wall force constant that was set as 0.5 for inner wall and 3.0 for outer wall in **Figure 3d&e**. In **Figure 3f&g**, the inner wall force constant was set as 0.5 and outer wall force constant was set as 1.5, 2.0 2.5, or 3.0 in each simulation. d_{iw} is the distance between the wall and the cell center.

The change in the velocity of the cells is given by $d_{ri}(t)/dt$ and is dependent on the inherent velocity of the cells and the mobility μ.

$$\frac{\mathrm{d}\mathbf{r}_i(t)}{\mathrm{d}t} = v_0 \mathbf{n}_i(t) + \mu \sum_{j=1}^{N} \mathbf{F}(\mathbf{r}_i, \mathbf{r}_j). \tag{8}$$

At each time step the preferred direction of motion of the cells changes due to its environmental interactions and is given by,

$$\frac{\mathrm{d}\theta_i^{\mathbf{n}}(t)}{\mathrm{d}t} = \frac{1}{\tau} \arcsin\left(\left(\mathbf{n}_i(t) \times \frac{\mathbf{v}_i(t)}{|\mathbf{v}_i(t)|}\right) \cdot \mathbf{e}_z\right) \tag{9}$$

Here, v_i is the velocity vector and e_z is the unit vector perpendicular to the plane. The parameter $1/\tau$ determines the tendency of cell preferred direction to align with the velocity vector, which was set as 0.5 in all simulations. The total cell number in different patterns was set as 519, 487, 413 and 300 for the pattern D = 1, 0.75, 0.55, 0.35 respectively.

Cells in the patterns were generated at random locations with random directions of initial cellular velocity at the start of the simulation. To analyze the asymmetric cell alignment index in a pattern in the simulation, all the cell's polarization orientations were used to calculated the cell alignment angle and overall asymmetric alignment index. The force and polarization orientations per cell at different radial difference to pattern centers were analyzed to investigate the dynamic of force changes over the iteration time.

SUPPORTING FIGURES

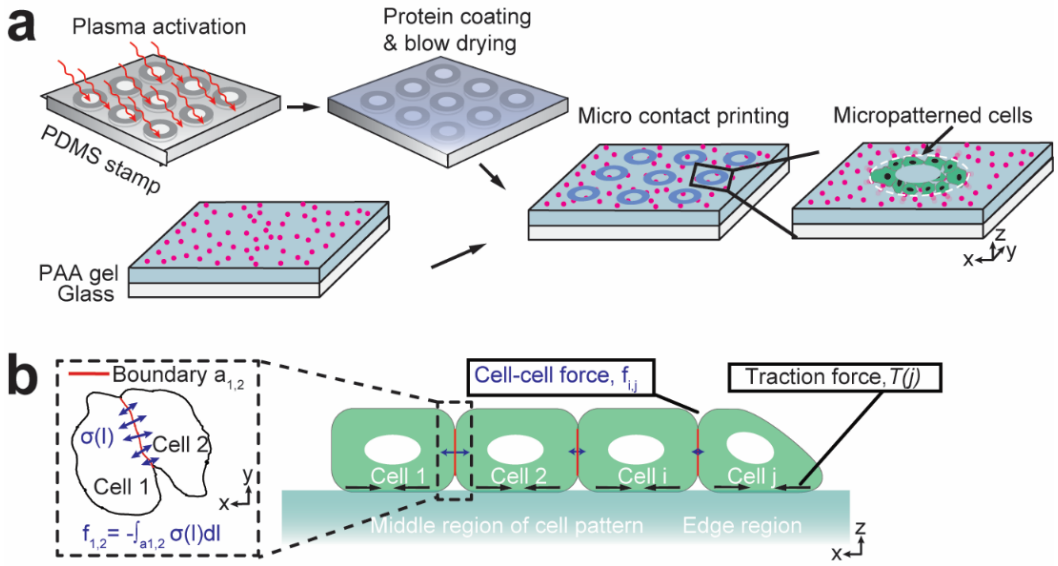

Figure S1. Micropatterned vascular cell sheet using micro-contact printing for cellular force and asymmetric cell alignment analysis. (**a**) A schematic illustrating the experimental procedures for micropatterned vascular cell sheet on mechanical-force sensing PAA hydrogel. (**b**) A schematic showing the model of traction and cell-cell forces in a vascular sheet. Intercellular forces were calculated by integrating internal stress distribution along the boundary between two neighboring cells.

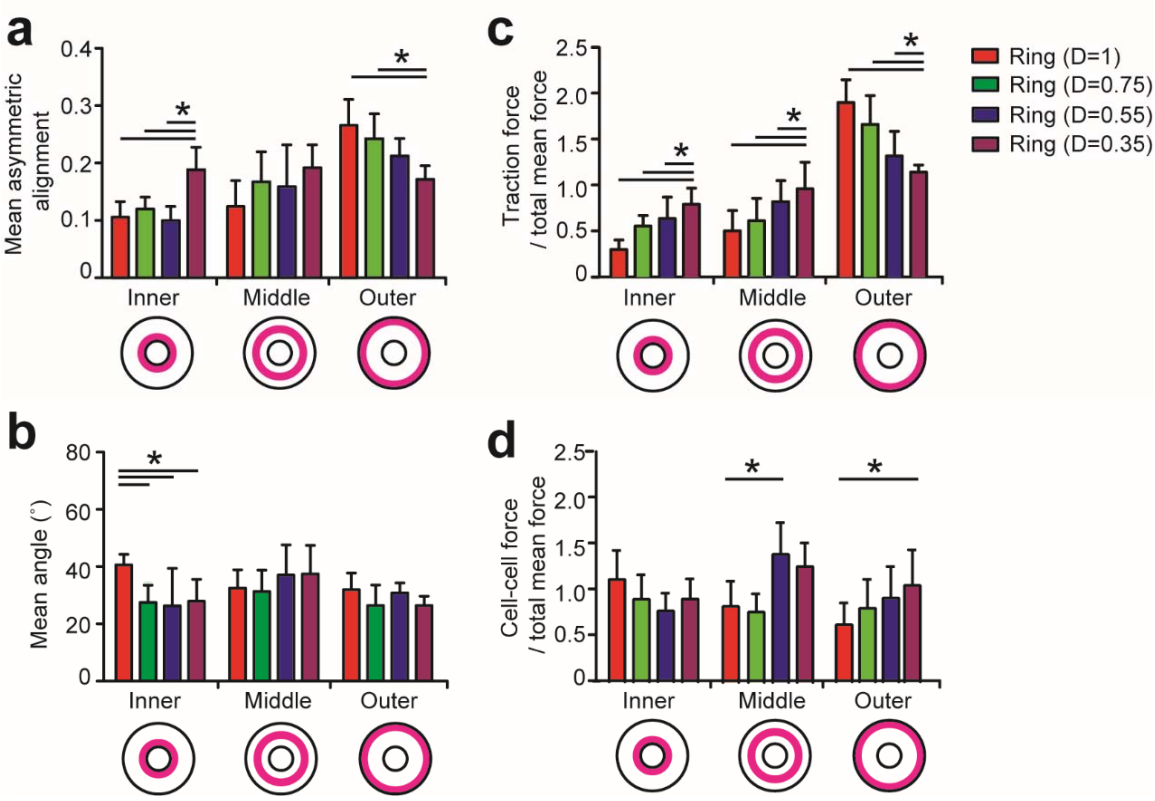

Figure S2. Distinct mechanical forces and cell arrangments in different geometric patterns. (**a**) Quantified mean asymmetric cell alignment and mean cell alignmnet angle (**b**) in differnt subregions within different ring patterns. (**c**) Quantified ratio of traction force and (**d**) ratio of cell-cell force in three subregions over total mean force within different ring patterns. P-values were calculated using the Student's paired sample t-test or one-way ANOVA. *, $P < 0.05$.

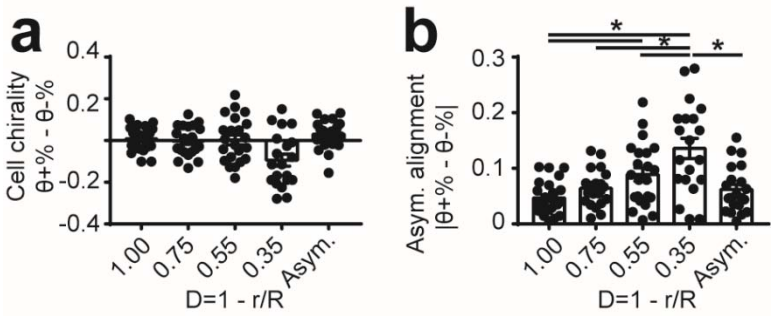

Figure S3. Cell chirality and asymmetric cell alignment analysis. (**a**) Cell chirality analysis of alignment angles reveals no obvious preference towards positive or negative angles in different micropatterns (D = 1, 0.75 and 0.55). Interestingly, negative cell chirality was observed in narrow rings (D = 0.35). Cell chirality was defined between -1 to 1 as the ratio difference of positive and negative cell alignment angles θ+% - θ-%. (**b**) Quantified asymmetric alignments of endothelial cells confined in different topographic ring-shapes. Asymmetric alignment index was defined between 0-1 as the absolute ratio difference of positive and negative cell alignment angles $|\theta^{+}\% - \theta^{-}\%|$. *P*-values were calculated using the one-way ANOVA. *, $P < 0.05$.

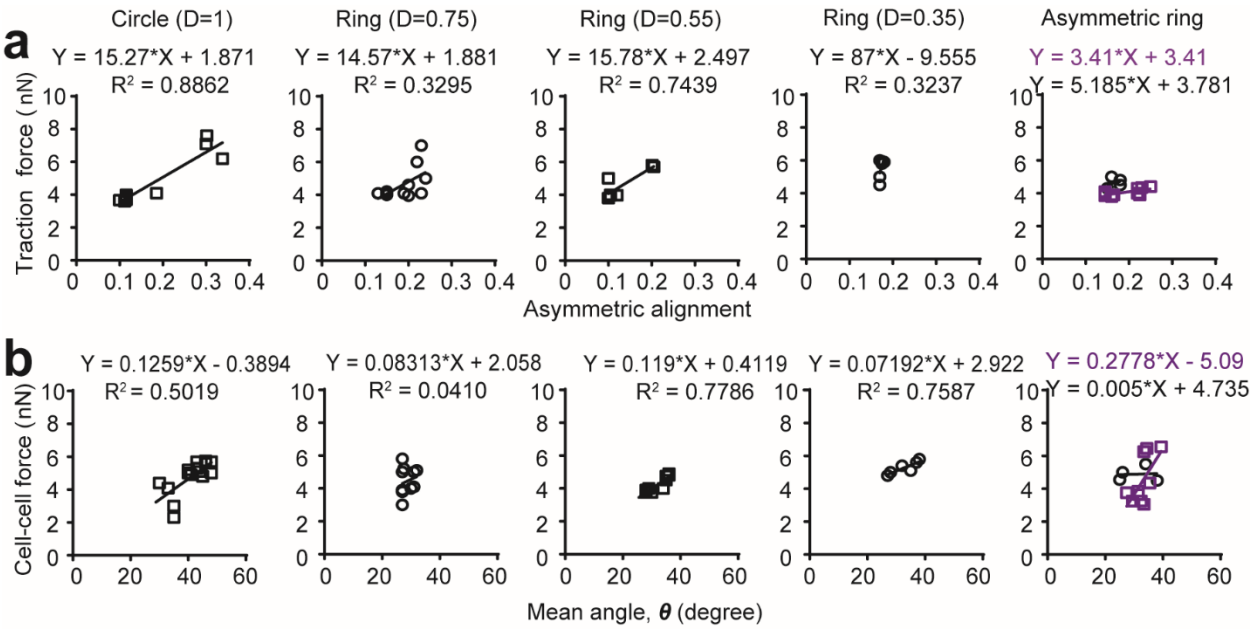

Figure S4. Correlation between mechanical force and cellular morphological feature. (**a**) Correlation of traction force and asymmetric cell alignment within different micropatterns. Note the strong dependence of radial asymmetric cell alignment on traction force. (**b**) Correlation of cell-cell force and mean angle within different ring patterns.

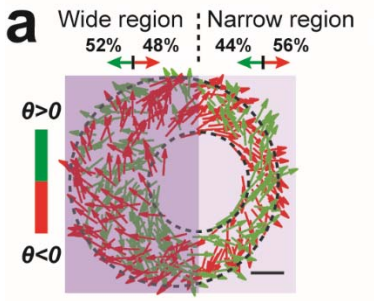

b

Region	Traction force (nN)		Cell-cell force (nN)		Asymmetric alignment		Cell chirality
	Mid.	Edge	Mid.	Edge	Mid.	Edge	
Wide	3.46	7.59	6.98	6.79	0.13	0.22	0.04
Narrow	5.92	5.89	5.39	5.30	0.17	0.16	-0.12
Overall	5.51		5.98		0.02		-0.02

Figure S5. Different mechanical forces and cell arrangments in annulus pattern. (**a**) Analysis of cell alignment in the micropatterned annulus vascular sheet. Note that the mean chirality for wide and narrow region is~ 0.04 and -0.12, respectively. (**b**) A summarized table to show the quantified mechanical force, asymmetric cell alignment and chirality in the wide and narrow regions in the annulus pattern. Note the increased traction force, asymmetric cell alignment and negative cell chirality in narrow regions.

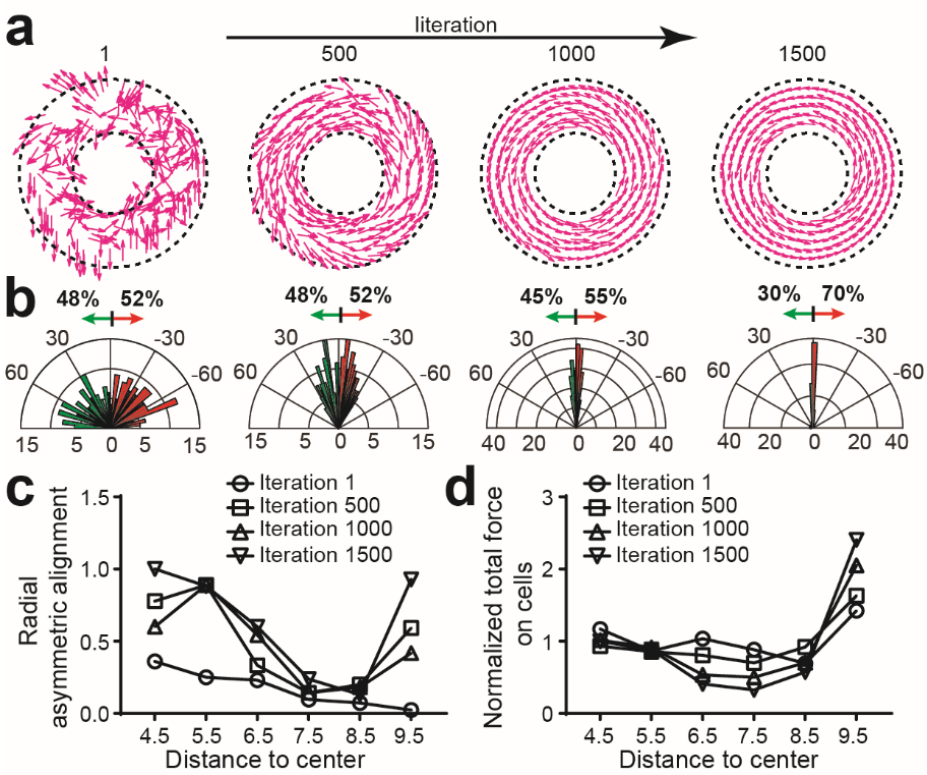

Figure S6. Asymmetric cell alignment and force profiles in CAM simulations. (**a**) Snapshots at iteration time of 1, 500, 1000 and 1500 were shown in a ring pattern (D = 0.55). The red arrow represents the polarization angle for each cell. (**b**) Histogram of the mean alignment angles at different iteration time in a ring pattern (D = 0.55). Noted the random initial state and asymmetric cell alignment forming over iteration time. (**c**) Quantified radial asymmetric cell alignment index and (**d**) quantified mean force of cells at different radial positions in a ring pattern (D = 0.55). The radial distance to the center of the ring pattern was set as a non-dimensional value in simulation. Noted the higher force and asymmetric alignment index in the regions close to pattern edges over the iteration.

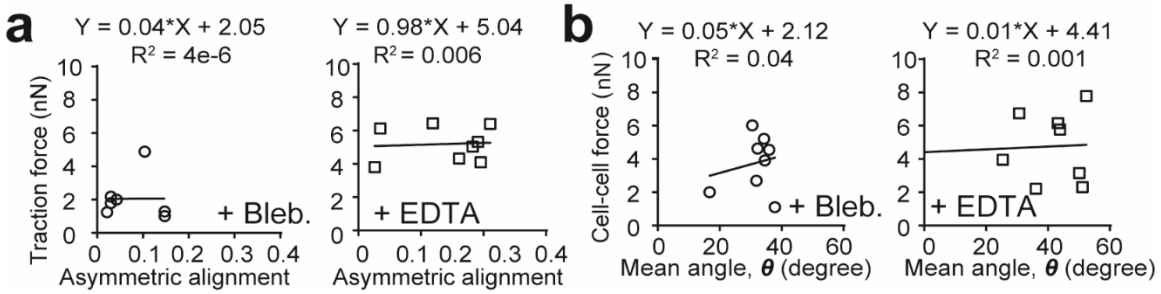

Figure S7. Correlations between mechanical force and asymmetric cell alignment under pharmacological treatments. (**a**) Correlation of traction force and radial asymmetric cell alignment and (**b**) cell-cell force and mean angle with blebbistatin and EDTA treatments that inhibit traction and cell-cell forces. Note the weak dependence of cell chirality and mean angle on mechanical force after pharmacological treatments.